

A robust approach for time-bin encoded photonic quantum information protocols

Simon J. U. White,^{1,*} Emanuele Polino,^{*,1,†} Farzad Ghafari,^{1,‡} Dominick J. Joch,¹ Luis Villegas-Aguilar,¹ Lynden K. Shalm,² Varun B. Verma,² Marcus Huber,^{3,4} and Nora Tischler^{1,§}

¹Centre for Quantum Dynamics and Centre for Quantum Computation and Communication Technology Griffith University Yuggera Country Brisbane Queensland 4111 Australia

²National Institute of Standards and Technology 325 Broadway Boulder Colorado 80305 USA

³Atominstytut Technische Universität Wien Stadionallee 2 1020 Vienna Austria

⁴Institute for Quantum Optics and Quantum Information (IQOQI) Austrian Academy of Sciences Boltzmanngasse 3 1090 Vienna Austria

Quantum states encoded in the time-bin degree of freedom of photons represent a fundamental resource for quantum information protocols. Traditional methods for generating and measuring time-bin encoded quantum states face severe challenges due to optical instabilities, complex setups, and timing resolution requirements. Here, we leverage a robust approach based on Hong-Ou-Mandel interference that allows us to circumvent these issues. First, we perform high-fidelity quantum state tomographies of time-bin qubits with a short temporal separation. Then, we certify intrasystem polarization-time entanglement of single photons through a nonclassicality test. Finally, we propose a robust and scalable protocol to generate and measure high-dimensional time-bin quantum states in a single spatial mode. The protocol promises to enable access to high-dimensional states and tasks that are practically inaccessible with standard schemes, thereby advancing fundamental quantum information science and opening applications in quantum communication.

Photonic quantum technologies rely on the capability to manipulate and measure quantum states of photons [1, 2]. Among the variety of photonic degrees of freedom that can be used to encode quantum states, one of the most noise-resilient and reliable is time. This degree of freedom was first proposed by Franson to test quantum nonlocality [3]. Here, quantum states can be encoded using the arrival time of photons, i.e. time bins, which offer an infinite Hilbert space to encode information in high-dimensional states [4–7]. Time-bin states have been shown to be highly robust against turbulence and are suitable for long-distance transmissions in fibers [8–12], free-space interconnects [13–17], and ground-satellite links [18, 19]. These properties make time-bin encoding a promising choice for quantum communication [20–29] and may be the foundation for the future quantum internet [30–32].

An increasingly important challenge is the robust and efficient generation and measurement of time-bin encoded states. To date, the most common techniques are based on unbalanced interferometers followed by time-resolved detection [3, 33], using post-selection for the recombination after an interferometer, or active switching protocols [34]. Unfortunately, interferometric techniques can suffer from severe limitations, where large differences in interferometer arm lengths are required for detectors to resolve neighboring time bins. Although state-of-the-art superconducting single-photon detectors and electronics can reach a jitter and time resolution on the order of a few picoseconds [24, 35–38], standard technology and electronics available to most laboratories limit the overall time resolution to the order of nanoseconds. Consequently, the use of large unbalanced interferometers is often practically unavoidable. This leads to poor scalability in optical setups due to phase instabilities during long integration measurements, and impractical setups for high-dimensional states (requiring larger interferometers exacerbates these difficulties). Other time-bin measurement techniques do exist, such as those based on nonlinear optical interactions, including

pulse-shaping in conjunction with sum-frequency generation [39–42]. Alternatively, using both optical nonlinearity and interferometers allows one to resolve short time delays [43, 44]. These approaches, however, come at the cost of increased complexity and expense, limiting their suitability for most applications. To avoid the use of unbalanced interferometers, frequency-based techniques can be employed, but they only allow for particular measurements in the time-bin space, such as mutually unbiased bases [45]. As a result, the practical drawbacks of standard measurement techniques pose severe limitations on the robustness, feasibility, and accessible Hilbert space dimensionality of time-bin states used in real experiments.

In this work, we employ a measurement scheme based on Hong-Ou-Mandel (HOM) interference [46] that overcomes the intrinsic limitations present in standard approaches and enables different tasks. The HOM effect is based on the quantum interference between indistinguishable photons and is a building block for realizing interaction between photons in multi-photon protocols [47]. Here, we apply the HOM measurement scheme to harness time-bin quantum encoding in a robust way: That is, the scheme enables short temporal delays, manipulated by reliable, versatile, and low-noise setups. This allows us to advance time-bin based photonic information protocols in three core directions.

First, we provide an optical experiment, using time-bin qubits generated by intrinsically stable unbalanced interferometers. We demonstrate that the measurement approach is reliable and can be used to perform high-quality quantum-state tomography with an average fidelity between reconstructed and target states of $\langle F \rangle = 99.55 \pm 0.07\%$. Next, we use the versatility of the protocol to perform a noncontextuality test for the intrasystem entanglement between the polarization and time degrees of freedom of single photons. Violating a Bell-like inequality, we unambiguously demonstrate the presence of entanglement between these degrees of freedom. Finally,

we propose a scheme, based on quantum walk dynamics, to generate high-dimensional time-bin quantum states. The proposed scheme allows for arbitrary measurements, which are increasingly difficult in high dimensions, enabling high-dimensional quantum communication protocols and nonlocality tests.

By improving the robustness, versatility, and accessible dimensionality of time-bin encoded states, this work represents an advance toward scalable quantum technology protocols.

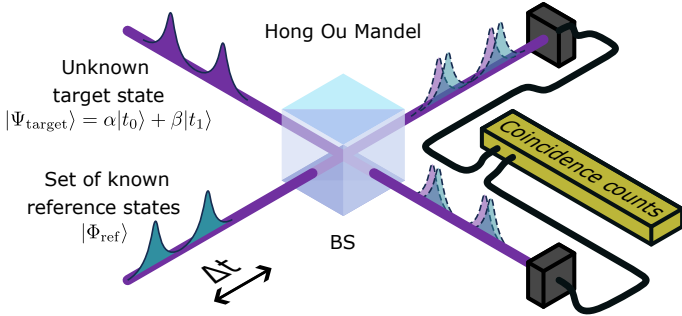


Figure 1. **Conceptual scheme of HOM-based measurement.** The unknown target photon is measured by means of a known and controlled reference photon via HOM interference at a beam splitter (BS). From the coincidence counts, one can deduce the projection value.

Measurement scheme — The goal here is to use HOM interference to perform arbitrary projective measurements on an unknown target time-bin encoded quantum state $|\Psi_{\text{target}}\rangle$. Suppose the temporal wavefunction of a reference state is prepared in the state $|\Phi_{\text{ref}}\rangle$. Then, one performs a HOM experiment (see Fig. 1), interfering the two photons on a beam splitter (BS). The probability P_{ab} of measuring a coincidence event between the two outputs of the BS (anti-bunching), given that the photons are indistinguishable in all other degrees of freedom besides time and path, will depend on their overlap [46, 48], which in the case of pure reference state reads:

$$P_{ab} = \frac{1 - |\langle \Phi_{\text{ref}} | \Psi_{\text{target}} \rangle|^2}{2}. \quad (1)$$

One can realize arbitrary projections on a target (pure or mixed) photon by preparing a suitable (pure) reference photon and performing a HOM interference experiment. This kind of measurement is general and can be applied, in principle, to any photonic degree of freedom (for polarization and hybrid polarization-time states see Refs. [49–51]). Furthermore, different kinds of light sources can be used as a reference [49].

The minimum delay required in principle to resolve two time bins is limited only by the coherence length of the employed single photons. This minimal delay maximizes the robustness against noise during preparation, transmission, and measurement.

Although we focus on time-bin qubits in the first part of this work, the scheme can be directly generalized to arbitrary high-dimensional states. This is because rela-

tion (1) provides information on the overlap between photonic states, independently of their dimensionality. Hence, given the ability to prepare arbitrary reference states, the measurement scheme applies to any time-bin encoded quantum state (qudit).

Measurements of time-bin qubits — To verify the experimental performance of the scheme depicted in Fig. 1, we carry out an experiment using single photons (see Fig. 2). A pair of photons is generated using spontaneous parametric down-conversion (SPDC) by a pulse at time t_0 , in a separable state of time and polarization $|t_0\rangle_s |H\rangle_s \otimes |t_0\rangle_i |V\rangle_i$, where the subscripts indicate signal and idler photon, respectively (see Supplemental Material).

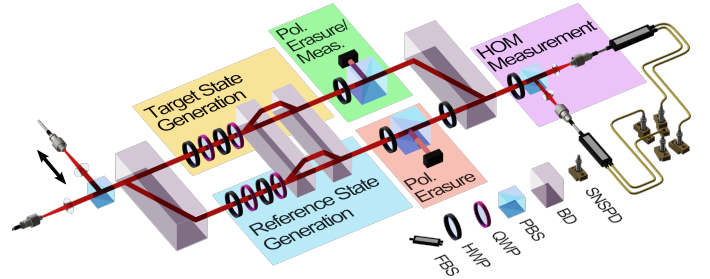


Figure 2. **Experimental setup.** The states of two single photons are independently encoded using their polarization, and are then mapped into time-polarization states (yellow and blue panels). The polarization is either erased for the tomography experiment, using a PBS (red and green panels), or measured to verify intrasystem entanglement using a suitably rotated HWP and a PBS (green panel). Target and reference photons are recombined to perform projection via HOM interference (purple panel); coincidences are recorded using SNSPDs and counting modules. HWP, half-waveplate; QWP, quarter-waveplate; PBS, polarizing beam splitter; BD, beam displacer; SNSPD, superconducting-nanowire single-photon detector; FBS, fiber-beam splitter.

The polarization of two photons is independently manipulated using waveplates along their respective paths (yellow and blue panels in Fig. 2), preparing the arbitrary polarization state $|\Psi\rangle = \cos(\alpha) |H\rangle + e^{i\phi} \sin(\alpha) |V\rangle$, which is then directly mapped to time-bin encoding by means of an intrinsically stable asymmetric interferometer, based on beam displacers (BDs). Photons in one polarization state experience a temporal delay $\simeq 8$ ps (state $|t_1\rangle$), relative to the undisplaced polarization (state $|t_0\rangle$). After the asymmetric interferometer the state of each photon will be entangled in the polarization and time degrees of freedom of the same particle. To generate pure time-bin qubits, the polarization information is erased by a fixed half-waveplate (HWP) at 22.5° followed by a polarizing beam splitter (PBS). The complete evolution probabilistically maps (with probability $p = 1/2$) the polarization to pure time-bin qubits for each photon: $|\Psi\rangle = |t_0\rangle \otimes (\cos(\alpha) |H\rangle + e^{i\phi} \sin(\alpha) |V\rangle) \implies (\cos(\alpha) |t_0\rangle + e^{i\phi} \sin(\alpha) |t_1\rangle) \otimes |H\rangle$.

To perform HOM measurements, the photons are recombined in a single path and, after a final HWP at 22.5° , interfere in a final PBS.

To demonstrate tomography of the time-bin encoded qubits using the HOM scheme, we reconstruct a num-

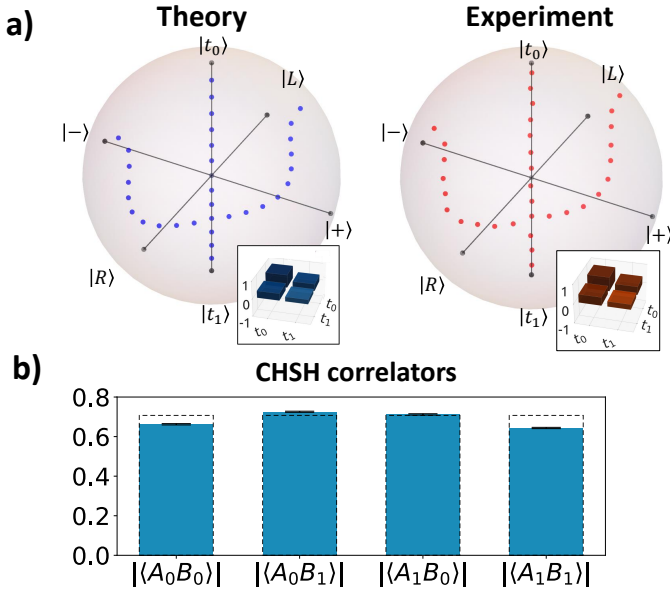


Figure 3. **Experimental results.** **a)** Experimentally reconstructed mixed states (red) and theoretical expectations (blue) on the Bloch sphere. Insets: Examples for real parts of density matrices. **b)** Expectation values of the correlators measured for the noncontextuality test of single-photon time-polarization hybrid entangled states. Dashed lines: ideal values for a singlet state and optimal measurements. Error bars are estimated assuming Poissonian statistics.

ber of (approximately) pure and mixed states. First, we prepare 15 states, including the six mutually unbiased bases (MUBs) states and nine randomly sampled pure states, and perform tomographic reconstruction. Furthermore, we prepared 33 states with varying amounts of mixture, as depicted in Fig. 3 a). To generate the necessary mixture, we prepared pairs of pure states and switched between them periodically throughout the measurement. For each tomography, we prepare the reference photon in the six states of the three MUBs. This measurement set is over-complete, and one can also use a smaller set using different strategies (see Supplemental Information I). We then reconstruct the target state using standard maximum likelihood estimation [52]. For both pure and mixed states, we obtained a mean experimental fidelity [53] of $\langle F^{\text{exp}} \rangle = 0.9955 \pm 0.0007$ with respect to theoretical targets (see the Supplemental Material for individual fidelities). *Noncontextuality test for hybrid entangled polarization-time single photon state* — Intrasystem entanglement describes the entanglement between different degrees of freedom of a single particle [54]. These hybrid entangled states [55–57] hold promise for efficient high-dimensional quantum information schemes [58], as they can also be used to enlarge the overall Hilbert space of a single particle. For photons, this kind of entanglement has been experimentally demonstrated through nonclassicality tests in orbital angular momentum (OAM)-polarization states [59–65] and path-polarization [66, 67].

Our approach allows us to extend these kind of demonstrations, by performing a nonclassicality test that unambiguously shows the presence of intrasystem entanglement in the time-polarization degrees of freedom through the violation of a Bell-like inequality.

As described in the previous section, our experimental setup naturally produces time-polarization entangled single-photon states. For instance, if one prepares the photon in the $|-\rangle$ polarization, the single photon entangled state (before the polarization erasure) is:

$$|\psi\rangle = \frac{1}{\sqrt{2}}(|H\rangle|t_0\rangle - |V\rangle|t_1\rangle). \quad (2)$$

In the realm of quantum mechanics, entanglement and nonlocality are distinct yet interconnected phenomena [68–70]. Although the intrasystem entangled state in Eq. (2) cannot generate nonlocality due to the lack of spatial separation between measurements [71], it can give rise to a violation of classical noncontextual models [59, 72–74].

To demonstrate nonclassicality, and therefore certify time-polarization entanglement, we performed a Clauser Horne Shimony Holt (CHSH) [75] type test, measuring the quantity $|S| = |\langle A_0 B_0 \rangle - \langle A_0 B_1 \rangle + \langle A_1 B_0 \rangle + \langle A_1 B_1 \rangle|$. Here, the correlation terms $\langle A_x B_y \rangle$ are calculated from the two-outcome measurements A_x and B_y (with binary measurement choices x and y) performed on the time and polarization degrees of freedom, respectively. The relation $|S| \leq 2$ holds for any noncontextual classical model that describes the correlations between measurement outcomes. We carried out the time-bin measurements as described previously. To measure the polarization state of the single photons independently of the time, we adjusted the polarization erasure step (green region in Fig. 2) to instead perform projective measurements with the HWP and PBS.

After generating the state described in Eq. (2) and performing the optimal measurements on this state ($\{\sigma_z, \sigma_x\}$ for A, and $\{\frac{\sigma_x + \sigma_z}{\sqrt{2}}, \frac{\sigma_x - \sigma_z}{\sqrt{2}}\}$ for B), we obtain a value of $|S|^{\text{exp}} = 2.744 \pm 0.006$ (the error is estimated by considering the Poissonian fluctuations of the counts), without rescaling the counts for accidental coincidences or limited HOM visibility. This result indicates a violation of the noncontextual bound by over 100 standard deviations, unequivocally certifying the presence of intrasystem entanglement between the time and polarization degrees of freedom of the single photons.

Proposal for generating and measuring high-dimensional time-bin photonic states — Leveraging the measurement scheme demonstrated above, we also devise a procedure for generating and measuring high-dimensional quantum states, overcoming the standard practical limitations. The crucial aspect used for this task is that the HOM measurement maps any projective measurement along arbitrary high-dimensional qudits into the preparation of high-dimensional reference states.

Our proposal exploits an efficient probabilistic scheme to generate arbitrary high-dimensional quantum states via quantum walk (QW) dynamics [76], which has previously been realised in high-dimensional OAM states [77, 78] and with 2D walks in the transverse momentum [79].

The basic tool for this task is a one-dimensional, discrete-time QW [80, 81] involving two quantum systems: a walker and a coin. The QW dynamics (see Supplemental Material IV) can be exploited to prepare arbitrary qudit states in the walker space by choosing the optimal coin operations [76], thereby changing the polarization at each step. Such dynamics produce a high-dimensional entangled target state in the coin-walker Hilbert space. The final pure walker state is probabilistically produced after projecting the coin state onto a suitable basis. Indeed, it is always possible to optimize the set of polarization operations that maximizes fidelity with an arbitrary state and the success probability at the same time [76, 77]. Furthermore, there is evidence that the number of required steps grows only linearly with the dimension of the target state [76, 77].

Here, we consider the time degree of freedom of a photon as the walker, living in an infinite dimensional space H_w spanned by discrete “position states” i.e., time-bin states $\{|t_i\rangle_w\}$, with $i \in \mathbb{N}$. The coin then corresponds to the polarization state of the photon, in a two-dimensional space H_c whose basis states, $|\uparrow\rangle := |H\rangle$ and $|\downarrow\rangle := |V\rangle$, denote the “movement directions” of the walker (see Refs. [82–87] for experimental realizations of time-bin-based quantum walks).

This polarization-time QW can be realized in a robust and straightforward way using only waveplates and birefringent elements. The waveplates are used to generate arbitrary coin operations, and the birefringent elements introduce a relative temporal delay (larger than the coherence length of the photon), acting on the temporal degree of freedom according to the polarization value. Importantly, this implementation uses only a single spatial mode and requires no need for spatial interferometers at all. The coin projection can be implemented by a PBS, after which the arbitrary state in the time bin is generated (see Fig. 4 a). The limit on the achievable dimension is given by the length of the QW. Importantly, the time-bin state can be arbitrarily adjusted by only tuning the waveplates, making it considerably more practical than changing large spatial interferometric setups.

This scheme can be used for different tasks. One possible scenario is the preparation and measurement of a single photon in a high-dimensional state for general quantum communication. Here, the sender uses one QW to prepare the message state to be sent, while the receiver uses a second QW to prepare the reference state of the photon, which is used to measure the message. The reference photon could be the twin photon generated by an SPDC source, or a photon generated by a source electronically synchronized with the source generating the first photon. The rapid development of on-demand single-photon sources, such as quantum dots, has already enabled several time-bin-encoded demonstrations [88–93], and such sources represent promising candidates for implementing high-dimensional single-photon time-bin states within our approach.

A second scenario would be quantum key distribution (QKD), depicted in Fig. 4 b): A pair of time-bin entan-

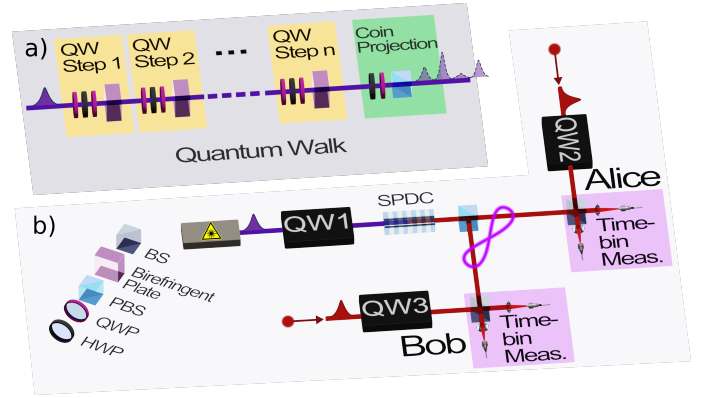


Figure 4. **Conceptual scheme of the proposal to create and measure high-dimensional states.** **a)** Through quantum walk (QW) dynamics, arbitrary high-dimensional time-bin states can be generated. **b)** Using the QWs as a building block, high-dimensional entangled states can be prepared, distributed, and measured. HWP, half-waveplate; QWP, quarter-waveplate; PBS, polarizing beam splitter; BS, beam splitter.

gled photons are shared among two measurement stations. The entangled state of the photons generated using an SPDC source can be engineered by suitably manipulating the pump in the time-bin degree of freedom. Here, a QW could be used to generate the time-bin state $|\Psi_p\rangle = \sum_{j=1}^n a_j |t_j\rangle$, where a_j are arbitrary coefficients and $\sum_{j=1}^n |a_j|^2 = 1$. Considering the cases where the probability of generating a pair of photons in a pulse is very low (so neglecting higher-order terms in the SPDC process), the following entangled state will be generated:

$$|\Psi\rangle = \sum_{j=1}^n a_j |t_j\rangle_s |t_j\rangle_i. \quad (3)$$

Then, the time-bin entangled photons are distributed to their respective measurement stations, where they can be measured using reference photons engineered by respective QWs (see Fig. 4 b) and Supplemental Material Fig. S3).

An attractive feature of this scheme is its scalability, as the number of optical elements scales linearly with the number of steps [76, 77]. Therefore, the effectively certifiable dimension of the state is fundamentally limited only by the ratio between the pump pulse separation and the coherence length of the generated photons, and not by the time resolution of the detector.

The generation and measurement of high-dimensional entangled states promises not only higher key rates, but indeed surpassing some of the fundamental bottlenecks of quantum communication, such as robustness of entanglement with respect to noise [94–96] or new ways of testing the foundations of quantum mechanics [97–100]. If the time bins can be temporally resolved by the detection apparatus, a significant benefit for QKD is the ability to perform multi-outcome measurements (those encoding the exchanged key), yielding $\log(d)$ bits for each coincident event. The test measurements can be implemented with the help of QW and would only require a small fraction of

total rounds, without the usual restriction of unbalanced interferometers.

Discussions — Time-encoded quantum states represent an extremely powerful tool for photonic quantum information tasks. Although several approaches have been developed to manipulate and measure these states, the standard techniques available are limited by instabilities and slow electronic devices. These shortcomings restrict the practicality and, therefore, the potential of time-bin encoding.

In this work, we used a scheme based on HOM interference to overcome some of these limitations and perform proof-of-principle experiments that highlight the versatility and high fidelity of this measurement approach. The scheme enables the use of time-bin qudits with minimal temporal delay between bins, limited only by the coherence time of the photons. With the use of femtosecond sources of single photons, one could extend this technique to create states with minimal delays between neighboring time bins, potentially surpassing the temporal resolution of existing detection technology.

This robust and reliable approach allowed us to detect the nonclassicality of intrasystem polarization-time entangled states of single photons. Furthermore, leveraging the demonstrated measurement method, we propose an intrinsically stable single-spatial-mode scheme for generating and measuring high-dimensional time-bin quantum states.

By enhancing the robustness and enlarging the accessible dimensionality, this work provides a step towards the scalable implementation of high-dimensional time-bin qudits as quantum information carriers.

Acknowledgments— This work was supported by ARC Grant No. CE170100012. L.V.-A. and D.J.J. acknowledge support by the Australian Government Research Training Program (RTP). We thank Sae-Woo Nam for supporting this work through his development of superconducting-nanowire single-photon detectors and Alex Pepper for helpful discussions and support with the experimental setup. M.H. acknowledges support from the Horizon-Europe research and innovation programme under grant agreement No. 101070168 (HyperSpace).

* These authors contributed equally to this work

† e.polino@griffith.edu.au

‡ f.ghafari@griffith.edu.au

§ n.tischler@griffith.edu.au

- [1] S. Slussarenko and G. J. Pryde, *Applied Physics Reviews* **6**, 041303 (2019).
- [2] F. Flamini, N. Spagnolo, and F. Sciarrino, *Reports on Progress in Physics* **82**, 016001 (2018).
- [3] J. D. Franson, *Physical Review Letters* **62**, 2205 (1989).
- [4] H. De Riedmatten, I. Marcikic, H. Zbinden, and N. Gisin, *Quantum Information & Computation* **2**, 425 (2002).
- [5] P. C. Humphreys, B. J. Metcalf, J. B. Spring, M. Moore, X.-M. Jin, M. Barbieri, W. S. Kolthammer, and I. A. Walmsley, *Physical Review Letters* **111**, 150501 (2013).
- [6] A. Martin, T. Guerreiro, A. Tiranov, S. Desiggnolle, F. Fröwis,

- N. Brunner, M. Huber, and N. Gisin, *Physical Review Letters* **118**, 110501 (2017).
- [7] M. Erhard, M. Krenn, and A. Zeilinger, *Nature Reviews Physics* **2**, 365 (2020).
- [8] W. Tittel, J. Brendel, H. Zbinden, and N. Gisin, *Physical Review Letters* **81**, 3563 (1998).
- [9] I. Marcikic, H. De Riedmatten, W. Tittel, H. Zbinden, and N. Gisin, *Nature* **421**, 509 (2003).
- [10] I. Marcikic, H. De Riedmatten, W. Tittel, H. Zbinden, M. Legré, and N. Gisin, *Physical Review Letters* **93**, 180502 (2004).
- [11] A. Cuevas, G. Carvacho, G. Saavedra, J. Cariñe, W. Nogueira, M. Figueroa, A. Cabello, P. Mataloni, G. Lima, and G. Xavier, *Nature Communications* **4**, 2871 (2013).
- [12] Q.-C. Sun, Y.-L. Mao, S.-J. Chen, W. Zhang, Y.-F. Jiang, Y.-B. Zhang, W.-J. Zhang, S. Miki, T. Yamashita, H. Terai, *et al.*, *Nature Photonics* **10**, 671 (2016).
- [13] T. Schmitt-Manderbach, H. Weier, M. Fürst, R. Ursin, F. Tiefenbacher, T. Scheidl, J. Perdigues, Z. Sodnik, C. Kurtsiefer, J. G. Rarity, *et al.*, *Physical Review Letters* **98**, 010504 (2007).
- [14] R. Ursin, F. Tiefenbacher, T. Schmitt-Manderbach, H. Weier, T. Scheidl, M. Lindenthal, B. Blauensteiner, T. Jennewein, J. Perdigues, P. Trojek, *et al.*, *Nature Physics* **3**, 481 (2007).
- [15] A. Fedrizzi, R. Ursin, T. Herbst, M. Nespola, R. Prevedel, T. Scheidl, F. Tiefenbacher, T. Jennewein, and A. Zeilinger, *Nature Physics* **5**, 389 (2009).
- [16] X.-M. Jin, J.-G. Ren, B. Yang, Z.-H. Yi, F. Zhou, X.-F. Xu, S.-K. Wang, D. Yang, Y.-F. Hu, S. Jiang, *et al.*, *Nature Photonics* **4**, 376 (2010).
- [17] F. Steinlechner, S. Ecker, M. Fink, B. Liu, J. Bavaresco, M. Huber, T. Scheidl, and R. Ursin, *Nature Communications* **8**, 15971 (2017).
- [18] G. Vallone, D. Dequal, M. Tomasin, F. Vedovato, M. Schiavon, V. Luceri, G. Bianco, and P. Villoresi, *Physical Review Letters* **116**, 253601 (2016).
- [19] J. S. Sidhu, S. K. Joshi, M. Gündoğan, T. Brougham, D. Lowndes, L. Mazzarella, M. Krutzik, S. Mohapatra, D. Dequal, G. Vallone, *et al.*, *IET Quantum Communication* **2**, 182 (2021).
- [20] J. Brendel, N. Gisin, W. Tittel, and H. Zbinden, *Physical Review Letters* **82**, 2594 (1999).
- [21] W. Tittel, J. Brendel, H. Zbinden, and N. Gisin, *Physical Review Letters* **84**, 4737 (2000).
- [22] N. Gisin and R. Thew, *Nature Photonics* **1**, 165 (2007).
- [23] T. Zhong, H. Zhou, R. D. Horansky, C. Lee, V. B. Verma, A. E. Lita, A. Restelli, J. C. Bienfang, R. P. Mirin, T. Gerrits, *et al.*, *New Journal of Physics* **17**, 022002 (2015).
- [24] N. T. Islam, C. C. W. Lim, C. Cahall, J. Kim, and D. J. Gauthier, *Science Advances* **3**, e1701491 (2017).
- [25] D. Cozzolino, B. Da Lio, D. Bacco, and L. K. Oxenløwe, *Advanced Quantum Technologies* **2**, 1900038 (2019).
- [26] E. Fitzke, L. Bialowons, T. Dolejsky, M. Tippmann, O. Niki-forov, T. Walther, F. Wissel, and M. Gunkel, *PRX Quantum* **3**, 020341 (2022).
- [27] A. Bergmayr, F. Kanitschar, M. Pivoluska, and M. Huber, (2023), [arXiv:2308.04422 \[quant-ph\]](https://arxiv.org/abs/2308.04422).
- [28] R. Valivarthi, S. I. Davis, C. Peña, S. Xie, N. Lauk, L. Narváez, J. P. Allmaras, A. D. Beyer, Y. Gim, M. Hussein, *et al.*, *PRX Quantum* **1**, 020317 (2020).
- [29] W. Wen, Z. Chen, L. Lu, W. Yan, W. Xue, P. Zhang, Y. Lu, S. Zhu, and X.-s. Ma, *Physical Review Applied* **18**, 024059 (2022).
- [30] S. Wehner, D. Elkouss, and R. Hanson, *Science* **362**, eaam9288 (2018).
- [31] F. Xu, X. Ma, Q. Zhang, H.-K. Lo, and J.-W. Pan, *Reviews of Modern Physics* **92**, 025002 (2020).

- [32] E. Diamanti, H.-K. Lo, B. Qi, and Z. Yuan, *npj Quantum Information* **2**, 1 (2016).
- [33] H. Takesue and Y. Noguchi, *Optics Express* **17**, 10976 (2009).
- [34] F. Vedovato, C. Agnesi, M. Tomasin, M. Avesani, J.-Å. Larsson, G. Vallone, and P. Villoresi, *Physical Review Letters* **121**, 190401 (2018).
- [35] I. Esmail Zadeh, J. W. Los, R. Gourgues, V. Steinmetz, G. Bulgarini, S. M. Dobrovolskiy, V. Zwiller, and S. N. Dorenbos, *APL Photonics* **2**, 111301 (2017).
- [36] B. Korzh, Q.-Y. Zhao, J. P. Allmaras, S. Frasca, T. M. Autry, E. A. Bersin, A. D. Beyer, R. M. Briggs, B. Bumble, M. Colangelo, *et al.*, *Nature Photonics* **14**, 250 (2020).
- [37] G. G. Taylor, E. N. MacKenzie, B. Korzh, D. V. Morozov, B. Bumble, A. D. Beyer, J. P. Allmaras, M. D. Shaw, and R. H. Hadfield, *Applied Physics Letters* **121**, 214001 (2022).
- [38] H. Hao, Q.-Y. Zhao, Y.-H. Huang, J. Deng, F. Yang, S.-Y. Ru, Z. Liu, C. Wan, H. Liu, Z.-J. Li, *et al.*, *Light: Science & Applications* **13**, 25 (2024).
- [39] A. Pe’Er, B. Dayan, A. A. Friesem, and Y. Silberberg, *Physical Review Letters* **94**, 073601 (2005).
- [40] O. Kuzucu, F. N. Wong, S. Kurimura, and S. Tovstonog, *Optics Letters* **33**, 2257 (2008).
- [41] J. M. Donohue, M. Agnew, J. Lavoie, and K. J. Resch, *Physical Review Letters* **111**, 153602 (2013).
- [42] J.-P. W. MacLean, J. M. Donohue, and K. J. Resch, *Physical Review Letters* **120**, 053601 (2018).
- [43] F. Bouchard, D. England, P. J. Bustard, K. Heshami, and B. Sussman, *PRX Quantum* **3**, 010332 (2022).
- [44] F. Bouchard, K. Bonsma-Fisher, K. Heshami, P. J. Bustard, D. England, and B. Sussman, *Physical Review A* **107**, 022618 (2023).
- [45] K.-C. Chang, M. C. Sarihan, X. Cheng, P. Erker, A. Mueller, M. Spiropulu, M. D. Shaw, B. Korzh, M. Huber, and C. W. Wong, “Experimental high-dimensional entanglement certification and quantum steering with time-energy measurements,” (2023), [arXiv:2310.20694 \[quant-ph\]](https://arxiv.org/abs/2310.20694).
- [46] C.-K. Hong, Z.-Y. Ou, and L. Mandel, *Physical Review Letters* **59**, 2044 (1987).
- [47] F. Bouchard, A. Sit, Y. Zhang, R. Fickler, F. M. Miatto, Y. Yao, F. Sciarrino, and E. Karimi, *Reports on Progress in Physics* **84**, 012402 (2020).
- [48] J. C. Garcia-Escartin and P. Chamorro-Posada, *Physical Review A* **87**, 052330 (2013).
- [49] Y. Tsujimoto, R. Ikuta, K. Wakui, T. Kobayashi, and M. Fujiwara, *Physical Review Applied* **19**, 014008 (2023).
- [50] G. P. Temporão, P. Ripper, T. B. Guerreiro, and G. C. do Amaral, *Phys. Rev. A* **109**, 022402 (2024).
- [51] Y. Pilnyak, P. Zilber, L. Cohen, and H. S. Eisenberg, *Physical Review A* **100**, 043826 (2019).
- [52] D. F. James, P. G. Kwiat, W. J. Munro, and A. G. White, *Physical Review A* **64**, 052312 (2001).
- [53] R. Jozsa, *Journal of Modern Optics* **41**, 2315 (1994).
- [54] Y. Shen and C. Rosales-Guzmán, *Laser & Photonics Reviews* **16**, 2100533 (2022).
- [55] B. N. Simon, S. Simon, F. Gori, M. Santarsiero, R. Borghi, N. Mukunda, and R. Simon, *Physical Review Letters* **104**, 023901 (2010).
- [56] J. H. Eberly, X.-F. Qian, A. Al Qasimi, H. Ali, M. Alonso, R. Gutiérrez-Cuevas, B. J. Little, J. C. Howell, T. Malhotra, and A. Vamivakas, *Physica Scripta* **91**, 063003 (2016).
- [57] S. Azzini, S. Mazzucchi, V. Moretti, D. Pastorello, and L. Pavesi, *Advanced Quantum Technologies* **3**, 2000014 (2020).
- [58] A. Forbes and I. Nape, *AVS Quantum Science* **1**, 011701 (2019).
- [59] E. Karimi, J. Leach, S. Slussarenko, B. Piccirillo, L. Marrucci, L. Chen, W. She, S. Franke-Arnold, M. J. Padgett, and E. Santamato, *Physical Review A* **82**, 022115 (2010).
- [60] E. Karimi, F. Cardano, M. Maffei, C. de Lisio, L. Marrucci, R. W. Boyd, and E. Santamato, *Physical Review A* **89**, 032122 (2014).
- [61] M. McLaren, T. Konrad, and A. Forbes, *Physical Review A* **92**, 023833 (2015).
- [62] V. D’Ambrosio, G. Carvacho, F. Graffitti, C. Vitelli, B. Piccirillo, L. Marrucci, and F. Sciarrino, *Physical Review A* **94**, 030304 (2016).
- [63] G. Milione, T. A. Nguyen, J. Leach, D. A. Nolan, and R. R. Alfano, *Optics Letters* **40**, 4887 (2015).
- [64] D. Cozzolino, E. Polino, M. Valeri, G. Carvacho, D. Bacco, N. Spagnolo, L. K. Oxenløwe, and F. Sciarrino, *Advanced Photonics* **1**, 046005 (2019).
- [65] A. Suprano, D. Zia, M. Pont, T. Giordani, G. Rodari, M. Valeri, B. Piccirillo, G. Carvacho, N. Spagnolo, P. Senellart, *et al.*, *Advanced Photonics* **5**, 046008 (2023).
- [66] M. Michler, H. Weinfurter, and M. Żukowski, *Physical Review Letters* **84**, 5457 (2000).
- [67] B. Gadway, E. Galvez, and F. De Zela, *Journal of Physics B: Atomic, Molecular and Optical Physics* **42**, 015503 (2008).
- [68] R. F. Werner, *Physical Review A* **40**, 4277 (1989).
- [69] N. Brunner, N. Gisin, and V. Scarani, *New Journal of Physics* **7**, 88 (2005).
- [70] L. Villegas-Aguilar, E. Polino, F. Ghafari, M. T. Quintino, K. T. Laverick, I. R. Berkman, S. Rogge, L. K. Shalm, N. Tischer, E. G. Cavalcanti, *et al.*, *Nature Communications* **15**, 3112 (2024).
- [71] A. Khrennikov, *Foundations of Physics* **50**, 1762 (2020).
- [72] S. Kochen and E. P. Specker, *Journal of Mathematics and Mechanics* **17**, 59 (1967).
- [73] C. Budroni, A. Cabello, O. Gühne, M. Kleinmann, and J.-Å. Larsson, *Reviews of Modern Physics* **94**, 045007 (2022).
- [74] D. Paneru, E. Cohen, R. Fickler, R. W. Boyd, and E. Karimi, *Reports on Progress in Physics* **83**, 064001 (2020).
- [75] J. F. Clauser, M. A. Horne, A. Shimony, and R. A. Holt, *Physical Review Letters* **23**, 880 (1969).
- [76] L. Innocenti, H. Majury, T. Giordani, N. Spagnolo, F. Sciarrino, M. Paternostro, and A. Ferraro, *Physical Review A* **96**, 062326 (2017).
- [77] T. Giordani, E. Polino, S. Emiliani, A. Suprano, L. Innocenti, H. Majury, L. Marrucci, M. Paternostro, A. Ferraro, N. Spagnolo, *et al.*, *Physical Review Letters* **122**, 020503 (2019).
- [78] A. Suprano, D. Zia, E. Polino, T. Giordani, L. Innocenti, A. Ferraro, M. Paternostro, N. Spagnolo, and F. Sciarrino, *Advanced Photonics* **3**, 066002 (2021).
- [79] C. Esposito, F. Di Colandrea, F. Hoch, G. Carvacho, F. Cardano, N. Spagnolo, L. Marrucci, and F. Sciarrino, *Physical Review Research* **5**, 043025 (2023).
- [80] Y. Aharonov, L. Davidovich, and N. Zagury, *Physical Review A* **48**, 1687 (1993).
- [81] S. E. Venegas-Andraca, *Quantum Information Processing* **11**, 1015 (2012).
- [82] A. Schreiber, K. N. Cassemiro, V. Potoček, A. Gábris, P. J. Mosley, E. Andersson, I. Jex, and C. Silberhorn, *Physical Review Letters* **104**, 050502 (2010).
- [83] A. Schreiber, A. Gábris, P. P. Rohde, K. Laiho, M. Štefaňák, V. Potoček, C. Hamilton, I. Jex, and C. Silberhorn, *Science* **336**, 55 (2012).
- [84] J. Boutari, A. Feizpour, S. Barz, C. Di Franco, M. Kim, W. Kolthammer, and I. Walmsley, *Journal of Optics* **18**, 094007 (2016).
- [85] L. Lorz, E. Meyer-Scott, T. Nitsche, V. Potoček, A. Gábris, S. Barkhofen, I. Jex, and C. Silberhorn, *Physical Review Research* **1**, 033036 (2019).

- [86] A. Gherardi, S. De, A. Laneve, S. Barkhofen, J. Sperling, P. Mataloni, and C. Silberhorn, *Physical Review Research* **3**, 023052 (2021).
- [87] K. L. Fenwick, F. Bouchard, D. England, P. J. Bustard, K. Heshami, and B. Sussman, (2024), [arXiv:2404.02238 \[quant-ph\]](https://arxiv.org/abs/2404.02238).
- [88] H. Jayakumar, A. Predojević, T. Kauten, T. Huber, G. S. Solomon, and G. Weihs, *Nature Communications* **5**, 4251 (2014).
- [89] K. Takemoto, Y. Nambu, T. Miyazawa, Y. Sakuma, T. Yamamoto, S. Yorozu, and Y. Arakawa, *Scientific Reports* **5**, 14383 (2015).
- [90] L. Yu, C. M. Natarajan, T. Horikiri, C. Langrock, J. S. Pelc, M. G. Tanner, E. Abe, S. Maier, C. Schneider, S. Höfling, *et al.*, *Nature Communications* **6**, 8955 (2015).
- [91] J. Lee, B. Villa, A. Bennett, R. Stevenson, D. Ellis, I. Farrer, D. Ritchie, and A. Shields, *Quantum Science and Technology* **4**, 025011 (2019).
- [92] M. Anderson, T. Müller, J. Skiba-Szymanska, A. Krysa, J. Huwer, R. Stevenson, J. Heffernan, D. Ritchie, and A. Shields, *Physical Review Applied* **13**, 054052 (2020).
- [93] L. Carosini, V. Oddi, F. Giorgino, L. M. Hansen, B. Seron, S. Piacentini, T. Guggemos, I. Agresti, J. C. Loredó, and P. Walther, *Science Advances* **10**, eadj0993 (2024).
- [94] S. Ecker, F. Bouchard, L. Bulla, F. Brandt, O. Kohout, F. Steinlechner, R. Fickler, M. Malik, Y. Guryanova, R. Ursin, and M. Huber, *Physical Review X* **9**, 041042 (2019).
- [95] M. Doda, M. Huber, G. Murta, M. Pivoluska, M. Plesch, and C. Vlachou, *Phys. Rev. Appl.* **15**, 034003 (2021).
- [96] L. Bulla, M. Pivoluska, K. Hjørth, O. Kohout, J. Lang, S. Ecker, S. P. Neumann, J. Bittermann, R. Kindler, M. Huber, *et al.*, *Physical Review X* **13**, 021001 (2023).
- [97] T. Vértesi, S. Pironio, and N. Brunner, *Physical Review Letters* **104**, 060401 (2010).
- [98] D. Collins, N. Gisin, N. Linden, S. Massar, and S. Popescu, *Physical Review Letters* **88**, 040404 (2002).
- [99] A. Vaziri, G. Weihs, and A. Zeilinger, *Physical Review Letters* **89**, 240401 (2002).
- [100] A. C. Dada, J. Leach, G. S. Buller, M. J. Padgett, and E. Andersson, *Nature Physics* **7**, 677 (2011).

Supplementary Information for: A robust approach for time-bin encoded photonic quantum information protocols

Simon J. U. White,^{1,*} Emanuele Polino^{*,1,†} Farzad Ghafari,^{1,‡} Dominick J. Joch,¹ Luis Villegas-Aguilar,¹ Lynden K. Shalm,² Varun B. Verma,² Marcus Huber,^{3,4} and Nora Tischler^{5,§}

¹*Centre for Quantum Dynamics and Centre for Quantum Computation and Communication Technology, Griffith University, Yuggera Country, Brisbane, Queensland 4111, Australia*

²*National Institute of Standards and Technology, 325 Broadway, Boulder, Colorado 80305, USA*

³*Atominstytut, Technische Universität Wien, Stadionallee 2, 1020 Vienna, Austria*

⁴*Institute for Quantum Optics and Quantum Information (IQOQI), Austrian Academy of Sciences, Boltzmannngasse 3, 1090 Vienna, Austria*

⁵*Centre for Quantum Dynamics and Centre for Quantum Computation and Communication Technology, Griffith University, Yuggera Country, Brisbane, Queensland 4111, Australia*

I. DIFFERENT POSSIBLE HOM MEASUREMENT NORMALIZATION TECHNIQUES TO ESTIMATE THE ANTI-BUNCHING PROBABILITIES

To perform a quantum state tomography using HOM measurements, one must estimate the anti-bunching probability P_{ab} in Eq. (1) of the main text. Normalization from raw coincidence counts to retrieve the probability P_{ab} , can be performed in a number of ways, given that the setup described in the main text allows one to obtain both anti-bunching and bunching events in the experiment directly. Anti-bunching events refer to events where the two photons exit the beam splitter along two different output ports, while the bunching events are those where the photons exit the same output port (Fig. S1 a) and b), respectively).

In Fig. S1 c) we show a measured HOM dip and peak, corresponding to bunching and anti-bunching respectively, resulting from interference of two photons in the same time-bin state $|t_0\rangle$. The HOM visibility obtained for indistinguishable photons in our setup amounts to $V = 98.5 \pm 0.3\%$. In Fig. S1 d) we present an example of the data collected when interfering a time-bin superposition state $|+\rangle = (|t_0\rangle \pm |t_1\rangle)/\sqrt{2}$, with the state $|t_0\rangle$. Here, we observe two HOM dips with reduced visibility $V \simeq 0.5$, corresponding to the photon wavefunction split among two time bins.

* These authors contributed equally to this work

† e.polino@griffith.edu.au

‡ f.ghafari@griffith.edu.au

§ n.tischler@griffith.edu.au

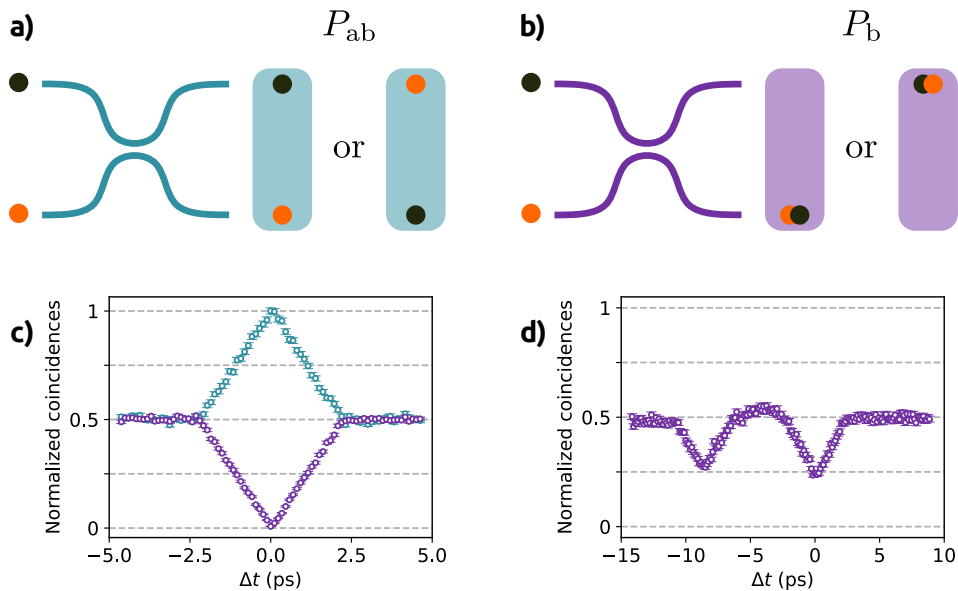


FIG. S1: **HOM measurement events** **a)** Anti-bunching events. **b)** Bunching events. **c)** Experimental HOM scan where both bunching (purple points) and anti-bunching (cyan points) are measured. The input photons are indistinguishable and are both in the state $|t_0\rangle$. The anti-bunching statistics, as a function of the relative delay between the two photons, is estimated using fiber-beam splitters connected to the outputs of the HOM beamsplitter. **d)** Anti-bunching events of the HOM scan with input photons with states $|t_0\rangle$ and $|+\rangle = (|t_0\rangle + |t_1\rangle)/\sqrt{2}$, respectively. Error bars are due to Poissonian statistics.

In our experiment, we chose to estimate the probabilities using anti-bunching coincidence counts only. To do this, in each measurement, we use the anti-bunching coincidences from both the target state (e.g., $|t_0\rangle$ for the time computational basis) and its orthogonal state ($|t_1\rangle$) as shown in Fig. S2 a). Consequently, we project upon all 6 MUBs states, two for each basis, for tomographic reconstruction of each state.

Two alternative methods to normalize the counts and retrieve the probability are briefly outlined below.

Fig. S2 b) depicts normalizing the anti-bunching terms by estimating the bunching terms via photon-number resolving detection. Photon-number resolution can be achieved with specialized detectors, such as transition edge sensors. Probabilistic photon-number resolution can be achieved using standard detectors following beam splitters (pseudo-photon-number resolution). In this way, one can perform both bunching and anti-bunching measurements simultaneously. However, to correctly estimate the bunching probability, a precise characterization of the beam-splitter splitting ratios and detector efficiencies is required.

Finally, another technique to estimate the anti-bunching probability could be to measure the anti-bunching counts far outside the center of the HOM dip, where the photons are always distinguishable independently of their time-bin state (Fig. S2 c).

In our experiment, we chose to estimate the overlaps using only anti-bunching coincidences to avoid the reliance on beam splitter characterization and the need to move the translation stage. The additional two fiber-beam splitters at the outputs of our setup were only used to check power fluctuations.

II. EXPERIMENTAL DETAILS

The single photon source is realized using a picosecond pulsed laser centered at 775 nm pumping a 1.5 cm-long periodically poled potassium titanyl phosphate (PPKTP) crystal. The type-II SPDC source produces photon pairs spectrally degenerate at 1550 nm.

The relative temporal delay between $|t_0\rangle$ and $|t_1\rangle$ introduced by the interferometer is around 8 ps, only slightly longer than the coherence time of the photons of ~ 2.3 ps. Two sets of waveplates control the polarization of each photon independently. The temporal delays define a two-dimensional Hilbert space spanned by the two time-bin states $\{|t_0\rangle, |t_1\rangle\}$.

A final BD recombines the two time-encoded photons into the same spatial mode, after which a polarization-based HOM experiment (equivalent to the one in Fig.(1) of the main text) is performed with a fixed HWP at 22.5° and a PBS. Coincidences are then measured by superconducting nanowire single-photon detectors (SNSPDs).

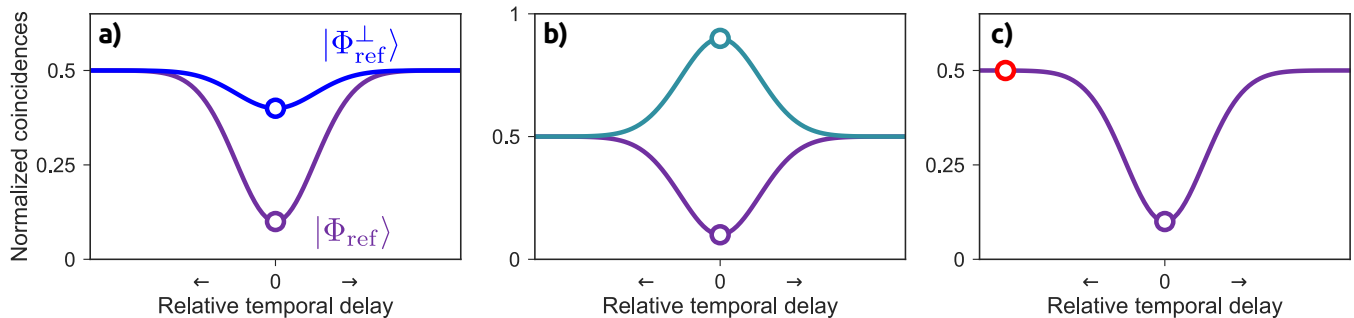


FIG. S2: **Conceptual normalization methods** Three methods for normalizing the anti-bunching coincidences of a HOM projection. The circles indicate the two measurements required to normalize the raw coincidences and obtain P_{ab} . **a)** Normalized anti-bunching counts (P_{ab}) corresponding to a projection with the reference state $|\Phi_{\text{ref}}\rangle$ (bottom, purple) and its orthogonal complement $|\Phi_{\text{ref}}^{\perp}\rangle$ (top, blue). Note that, inverting Eq.(1) of the main text, the relation between overlap between target and reference photons is given by: $|\langle\Phi_{\text{ref}}|\Psi_{\text{target}}\rangle|^2 = 1 - 2P_{ab}$. Hence, the two probabilities P_{ab} relative to the references $|\Phi_{\text{ref}}\rangle$ and $|\Phi_{\text{ref}}^{\perp}\rangle$, sum up to 0.5 in the zero-delay point. **b)** Both the bunching (top circle) and anti-bunching (bottom circle) counts of the same HOM projection. **c)** Anti-bunching counts of a projection at the center of the HOM dip (central circle) and far from the interference region (left circle). When the relative temporal delay is large enough, the two photons are always distinguishable, regardless of their time-bin state.

III. RESULTS OF QUANTUM STATE TOMOGRAPHIES

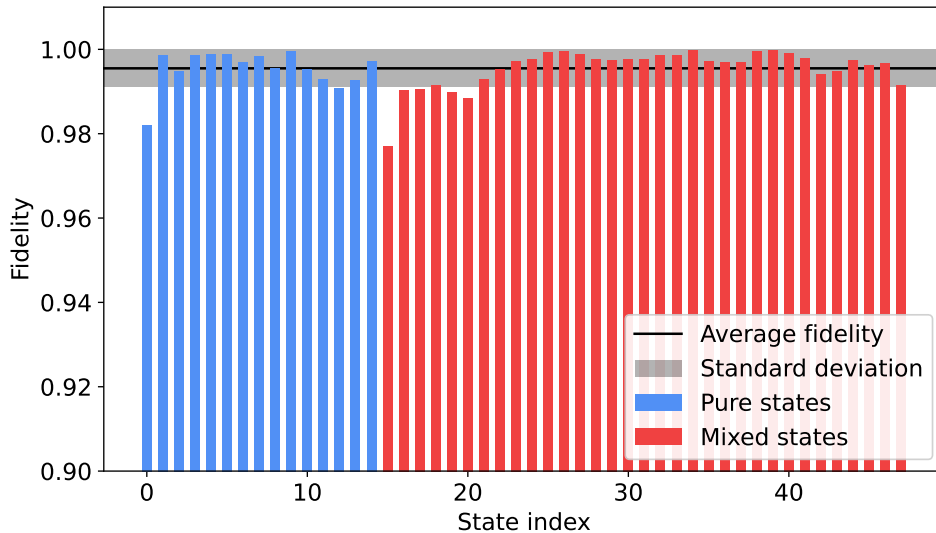


FIG. S3: **Experimental fidelities of the 48 individually reconstructed quantum states.**

In the barplot in Fig. S3 we present the values of the fidelities obtained for 48 generated and measured states (15 nominally pure and 33 mixed states). The density matrices of unknown states are recovered from the experimental probabilities using maximum likelihood estimation. Given the experimental density matrix ρ^{exp} , its fidelity with respect to the theoretical state ρ^{theo} is defined as: $F^{\text{exp}} = \text{Tr} \left[\sqrt{\sqrt{\rho^{\text{theo}}} \rho^{\text{exp}} \sqrt{\rho^{\text{theo}}}} \right]^2$.

We also directly depict the experimental quantum state tomographies obtained for the states belonging to the mutually unbiased basis (MUB) states in Figs. S4.

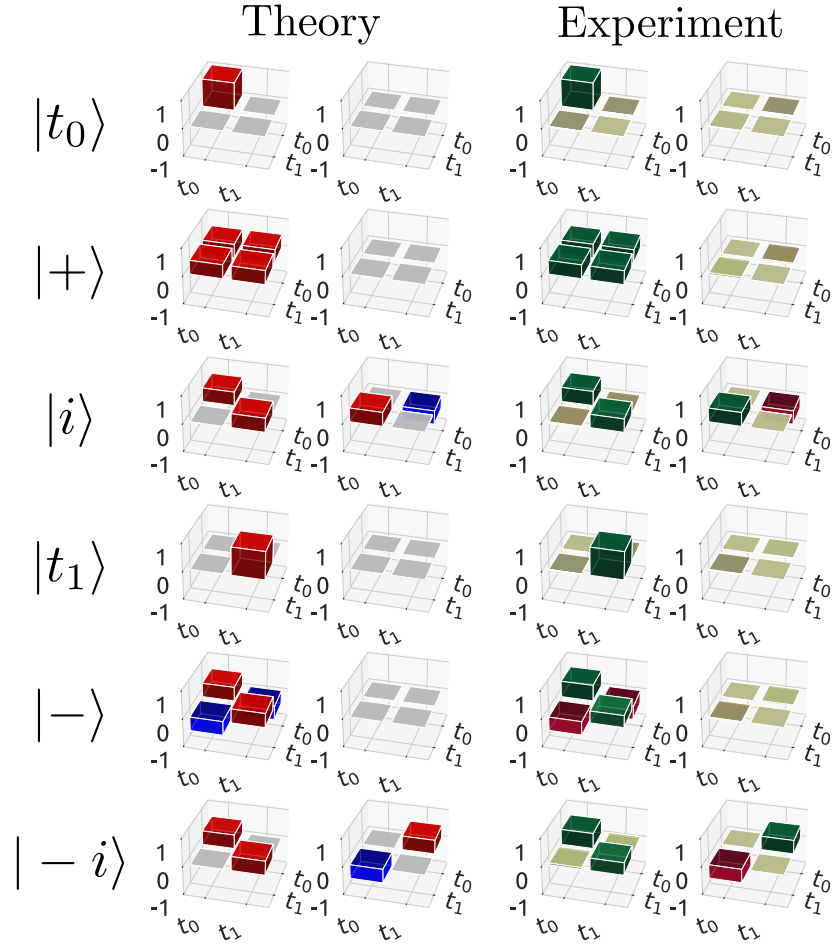


FIG. S4: **Tomography of mutually unbiased basis states.** Experimental results and theoretical comparison for the quantum state tomographies of the 6 states composing the MUBs. $|\pm\rangle \equiv (|t_0\rangle \pm |t_1\rangle)/\sqrt{2}$ and $|\pm i\rangle \equiv (|t_0\rangle \pm i|t_1\rangle)/\sqrt{2}$. For both theory and experimental tomographies, the real (left) and imaginary (right) parts are shown.

IV. DISCRETE-TIME QUANTUM WALK

The protocol proposed in the main text to generate arbitrary high-dimensional time-bin states is based on the dynamics of discrete-time quantum walks. A discrete-time quantum walk comprises two systems: a walker and a coin. The general quantum state of the walker will be $|\text{walker}\rangle = \sum_i c_i |t_i\rangle_w$, with $\sum_i |c_i|^2 = 1$, and the coin lives in a two-dimensional Hilbert space H_c with basis $\{|\uparrow\rangle := |H\rangle, |\downarrow\rangle := |V\rangle\}$. In our proposal, the coin is the polarization, and the walker lives in the time-bin space.

The complete dynamics of discrete-time QW is determined by a global evolution unitary operator U_t acting on the global system $|\Psi\rangle_{\text{tot}}$ at each step t . This unitary can be decomposed, at each step t , into a coin operator C_t acting solely on the polarization (coin) state, followed by a shift operator S_{cw} that controls the walker's movement depending on the coin state [1]:

$$S_{\text{cw}} = \sum_k |k\rangle\langle k|_w \otimes |\downarrow\rangle\langle\downarrow|_c + |k+1\rangle\langle k|_w \otimes |\uparrow\rangle\langle\uparrow|_c, \quad (1)$$

where k represents the position occupied by the walker in the time-bin space. As mentioned in the main text, the shift operator S_{cw} , which controls the movement of the walker depending on the coin state [1], can be realized in the proposal using a birefringent plate, which delays the time position of the photon according to its polarization.

The global evolution at step t is given by: $U_t = S_{\text{cw}}(C_t \otimes \mathbb{I}_w)$, where \mathbb{I}_w is the identity in walker space. Thus, the

final state after n steps will be

$$|\Psi\rangle_{\text{tot}}^n = \prod_{t=1}^n S_{\text{cw}}(C_t \otimes \mathbb{I}_w) |\Psi\rangle_{\text{tot}}^0, \quad (2)$$

where $|\Psi\rangle_{\text{tot}}^0$ is the initial state of the global system.

V. A POSSIBLE SCHEME FOR THE GENERATION AND MEASUREMENT OF HIGH-DIMENSIONAL ENTANGLED STATES USING AN SPDC SOURCE

The scheme theoretically proposed in the main text to generate and measure high-dimensional time-bin states can be used for entanglement-based quantum communication protocols and novel high-dimensional nonlocality tests.

We now theoretically describe a possible implementation, where photons are generated via a nonlinear crystal, as depicted in Fig. S5.

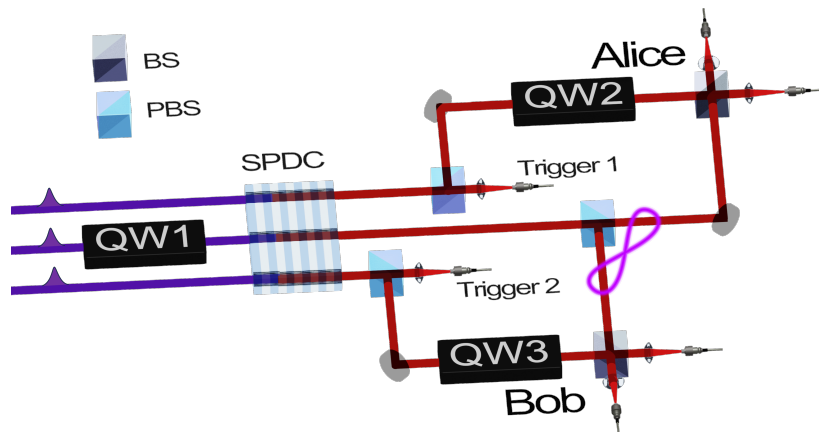


FIG. S5: **Experimental proposal.** Scheme for generating and measuring high-dimensional entangled states using spontaneous parametric down-conversion (SPDC) generating three pairs of photons. BS, beam splitter; PBS, polarizing beam splitter; QW, quantum walk.

In this scheme, the same crystal is pumped by three parallel beams from the same laser in three different positions to produce spectrally indistinguishable single photons via type-II SPDC. Two (out of six) photons are used to herald the existence of two other reference photons that are used for measuring the entangled photons (top and bottom paths). The entangled pair (middle path) is generated by temporally shaping the pump through quantum walk dynamics.

As described in the main text, this pump laser beam can be prepared by the quantum walk dynamics (QW1 in Fig. S5) in the arbitrary state $|\text{pump}\rangle = \sum_i c_i |t_i\rangle$, with $\sum_i |c_i|^2 = 1$ and $\{|t_i\rangle\}$ being the basis of time-bin space. After the nonlinear crystal, ignoring the higher-order terms, the state of the pair will be entangled and have the following form:

$$|\Psi\rangle = \sum_{i=1}^n a_i |t_i\rangle |t_i\rangle. \quad (3)$$

Once the entangled time-bin encoded photons are split according to their polarizations, they can be distributed among distant measurement stations, Alice and Bob. To measure the entangled pair with the HOM-measurement scheme, the heralded reference photons are prepared by the quantum walks QW2 and QW3, respectively.

It is worth mentioning that if deterministic sources reach a sufficiently high quantum efficiency, this method could be further simplified. In this scenario, Alice and Bob would generate their own reference photons synchronized with the laser pulse utilized for the entangled source at each measurement station.

[1] S. E. Venegas-Andraca, *Quantum Information Processing* **11**, 1015 (2012).